Report

Gas Pixel Detector Test and Analysis Report

Reference name	XIPE-IAPS-RP-0002
Version	1.1
Date	2017-03-27

Prepared by	Carmelo Sgrò, Michele Pinchera, Ettore Del Monte
Checked by	P. Soffitta
Approved by	P. Soffitta
Contact	carmelo.sgro@pi.infn.it

Document Change Record		
Date	Version	Changes
2017-02-13	1.0	Issue for MSR delivery
2017-03-27	1.1	Updated version including the results of the long duration leak test (sect. 5.3)

Applicable documents		
Reference	Reference name	Title
[AD1]	ESA-XIPE-EST-ENV-SP-001, Issue 1, Revision 1, 01/10/2015	XIPE Environmental Specification

Reference documents		
Reference	Reference name	Title
[RD1]	ESCC Basic Specification No. 25100 Issue 2 (2014)	SINGLE EVENT EFFECTS TEST METHOD AND GUIDELINES
[RD2]	R. Bellazzini, et al. in "X-ray polarimetry: A New Window in Astrophysics", Cambridge University Press, 269 – 274 (2010)	A polarimeter for IXO
[RD3]	R. Bellazzini et al., NIM A, 566, 552 – 562 (2006)	Direct reading of charge multipliers with a self-triggering CMOS analog chip with 105 k pixels at 50 μm pitch
[RD4]	L. Silvestrin et al., Proc. RADECS 2013 PB-9L 1/4, (2013)	Status and prospects of the SIRAD irradiation facility for radiation effects studies at LNL
[RD5]	S. Fabiani et al., ApJS 212 25 (2014)	The Imaging Properties of the Gas Pixel Detector as a Focal Plane Polarimeter
[RD6]	NASA-GSFC-STD-7000A 4/22/2013	General Environmental Verification Standard (Gevs)
[RD7]	VEGA (Arianspace) User's Manual, Issue 3/Revision 0, March 2006	
[RD8]	ECSS-E-ST-10-03C , June 2012	Space engineering Testing
[RD9]	D5002-TR-114 issue 1.0	OIA Polarimeter RGA test

List of Acronyms	
AOCS	Attitude and Orbit Control System
ASIC	Application Specific Integrated Circuit
CMOS	Complementary Metal-Oxide Semiconductor
DUT	Device Under Test
FEE	Front-End Electronics
F.O.V.	Field of view
GPD	Gas Pixel Detector
HIMAC	Heavy Ions Medical Accelerator in Chiba
LEO	Low Earth Orbit
LET	Linear Energy Transfer
LNL	Laboratori Nazionali INFN in Legnaro
SEE	Single Event Effect
SEL	Single Event Latch-up
SEU	Single Event Upset
TID	Total Ionising Dose
VLSI	Very Large Scale Integration

Contents

1 Introduction

The core of the XIPE mission is the Gas Pixel Detector (GPD) designed to detect the incident X-rays and measure energy, impact position and arrival time of each photon, as well as ejection direction of the photoelectron to be able to measure, on a statistical basis, polarization degree and angle of astrophysical sources.

The GPD is a gas detector, filled with a mixture whose main component is Dimethyl-Ether (DME), with a GEM as amplification stage and a finely subdivided ASIC as readout anode. The gas cell is sealed (no gas circulation/refilling system is necessary), it is composed of a 1 cm thick Macor walls glued on top of the GEM foil, with a Ti frame with a Be window on top and the ceramic package that contains the ASIC closing the bottom part of the cell. A schematic representation is shown in Figure 1:

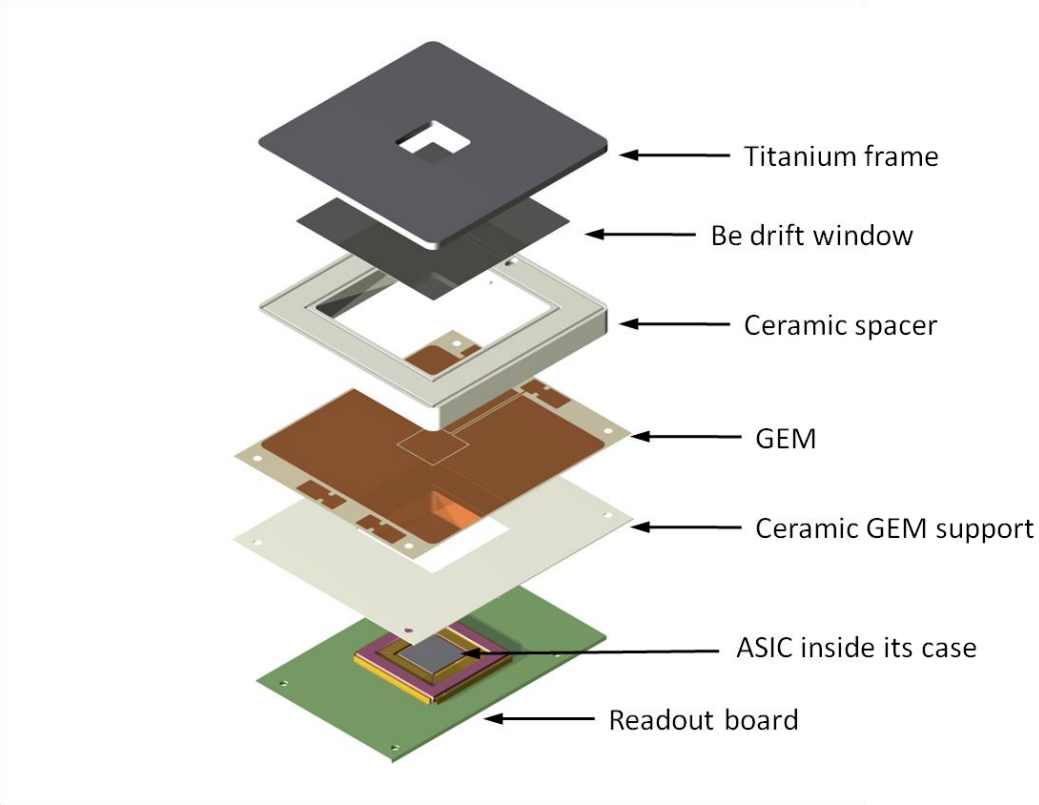

Figure 1: Schematic representation of GPD assembly.

Satellite-borne instrumentation is affected by the radiation damage due to the environment of charged and neutral particles in orbit. A detailed description of the effects of radiation damage is beyond the scope of this document. More information on the topic are e.g. in [RD1].

During the phase A study of the past ESA mission IXO[1], before submitting the XIPE proposal, we irradiated the Gas Pixel Detector (GPD) with an Fe beam of 500 MeV/nucleon energy at the Heavy Ions Medical Accelerator in Chiba (HIMAC) in Japan [RD2]. The total exposure was 1.7 x 10^4 Fe ions, corresponding to 42 years in space in a Low Earth Orbit (LEO). During the irradiation the GPD was powered on at the nominal voltage levels. The interaction of the Fe ions in the beam saturated the electronics and produced several secondary delta rays. We did not register any damage or performance loss in the detector [RD2]. A further

[1] http://sci.esa.int/ixo/

test was performed on the bare ASIC to verify its resistance to ionizing radiation and measure Single Event Latch-up and Single Event Upset cross section. This report describes in details this test and its result.

A prototype of the GPD, serial number 014, operated successfully for about 3 years, showing no significant degradation of performance, and underwent also thermal-vacuum and vibrational test. However, a direct measurement of the gas leak rate for an extended period was never performed, and it would be an additional proof of the readiness of the technology. For this reason, we are using that GPD prototype and check for possible leaks almost continuously for several weeks.

2 Radiation Damage

2.1 The XIPE radiation environment in orbit

From the XIPE Environmental Specification document [AD1], the baseline orbit for XIPE is a circular Equatorial Low Earth Orbit (LEO) with altitude of 550 km and inclination of 6°. The orbit was selected as a trade-off between the particle background flux and modulation (variation of the flux along the orbit) and the launcher capabilities and the duration of the passages above the ground station at Malindi.

2.2 Measurement of the sensitivity to latch-up and SEU

2.2.1 Motivation of the test

The front-end electronics (FEE) of the GPD is composed of a custom CMOS ASIC, produced by TSMC in Taiwan using a 0.18 μm CMOS VLSI technology and designed by INFN-Pisa [RD3]. Although the 0.18 μm VLSI technology is known to sustain high levels of radiation, the ASIC is not designed as a radiation hardened component for space applications. Consequently, as a step in the development path of the GPD, during the XIPE Assessment Study we irradiated the ASIC to measure the sensitivity to single event effects, in particular Single Event Latch-up (SEL) and Single Event Upset (SEU), and the resistance to the Total Ionising Dose (TID). We performed this irradiation at the SIRAD facility in the Laboratori Nazionali INFN in Legnaro (LNL) near Padova (Italy).

2.2.2 The SIRAD irradiation facility

As described in [RD4], the SIRAD irradiation facility is located at the +70° beam line (experimental Hall 1) of the Laboratori Nazionali INFN of Legnaro. The facility is connected to the Tandem-XTU electrostatic Van de Graaf accelerator and to the ALPI linear superconducting post-accelerator. The characteristics of the ion beams used in the irradiation of the XIPE ASIC are listed in Table 1.

Table 1: Characteristics of the ion beams used during the irradiation.

Ion	Rotation angle [deg]	Surface LET in Si [MeV cm^2 mg^{-1}]	Total Fluence [cm^{-2}]	Sum of the Total Ionising Dose [krad]
19F	0	3.9	3.42×10^8	21.4
19F	30	4.5	2.54×10^8	18.3
19F	45	5.5	2.13×10^8	18.8
35Cl	0	12.7	1.06×10^8	21.5
35Cl	45	18.0	4.10×10^7	11.8
79Br	0	41.9	9.21×10^7	61.8
79Br	30	48.4	7.87×10^7	61.0
79Br	45	59.3	6.38×10^7	60.6
127I	0	65.4	2.07×10^8	216.8

127I	45	92.5	6.56×10^7	97.2
			Total	589.4

As described in [RD4], the facility is equipped with a cylindrical irradiation chamber, with a diameter and length of 80 cm. A whole side opens like a large drawer, allowing easy access to the sample holder, which is mounted on the sliding floor. By opening the chamber everything inside slides out completely, thus providing tabletop-like working conditions. A picture of the irradiation chamber, sample holder and device under test (DUT) is shown in Figure 1. The sample holder can be displaced horizontally (over a 30 cm total length) and vertically (over 14 cm) using two DC motor stages, with a precision of 10 μm over both movements. A third motor stage can rotate the sample holder along the vertical axis with an angular excursion of 80° and better than 1° precision, thus allowing one to change the incident angle of beam on the DUTs. In this way the effective LET of the incident ion can be easily varied as ~1 / cos(θ) with θ rotation angle. The fluence is reduced of cos(θ) correspondingly.

An additional support frame ("fixed frame") is placed immediately upstream of the sample holder, and can be moved only along the horizontal direction. This frame hosts silicon diodes for online beam monitoring and diagnostics and a laser for target alignment.

As specified in [RD4], the uniformity of the ion beam is better than 10% over the 25 mm × 25 mm irradiation area.

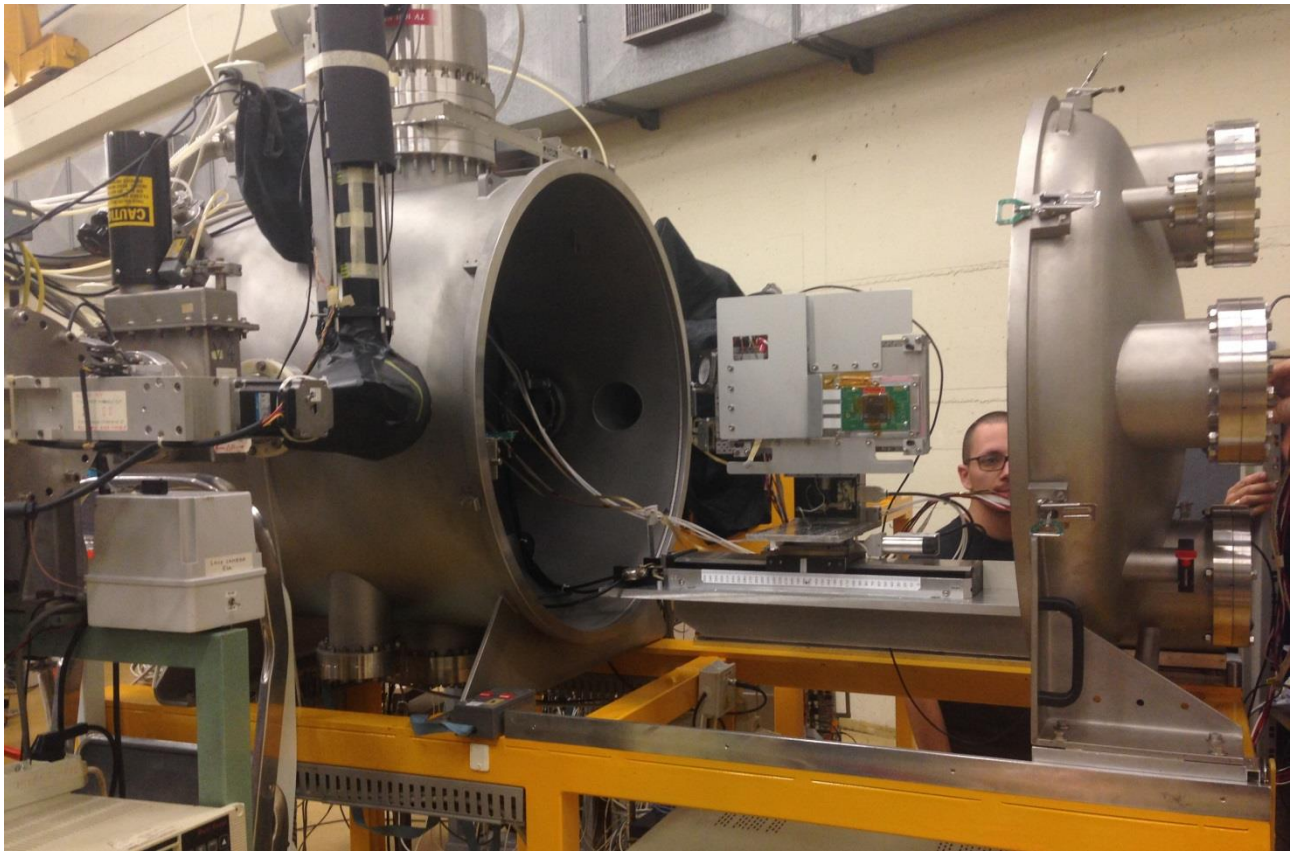

Figure 1: Irradiation chamber of the SIRAD facility, sample holder and DUT.

2.2.3 Experimental set-up

It is worth remarking here that in this test we irradiated only the ASIC, not the whole GPD.

The irradiation aims at measuring the ASIC cross section of latch-up, i.e. the sudden increase of the supply current due to the interaction of a charged particle, and of SEU, i.e. the bit flip produced by the interaction of a charged particle.

In order to monitor the power supply currents of the ASIC and detect the latch-up events, we designed and produced a custom acquisition board, based on the Arduino platform. The board measures the ASIC currents using a shunt resistor and an integrated circuit made by Texas Instruments (INA301A3-Q1). This equipment measures the current continuously, and compares it with a programmable threshold. The circuit sends an "Alert" signal to the Arduino as soon as one of the currents exceeds the threshold. Arduino can switch off the power supply with a typical reaction time of about 100 µs. The ASIC is powered on again after an idle time of 5 s. An internal counter (one per power line) is incremented and its value is sent to the control PC. The SEU can affect the ASIC in two different mechanisms:

1) The bit flip in the memory registers (24 bit) where the configuration is stored. To measure the cross-section of this type of SEU, we read the content of the configuration memory registers and compare it with the loaded string;
2) The bit flip of the token which is used to select the pixel in the analogue chain to measure the pulse height. To find the cross-section of this SEU, we continuously measured the value of the pulse height of the whole chip (~105k channels) using 8 analog lines and recording the events with a value greater than a user selectable number of standard deviations from the average value ("pedestal scan").

To measure the ASIC sensitivity to both types of SEU specified above we used the Data Acquisition system (DAQ) of the GPD.

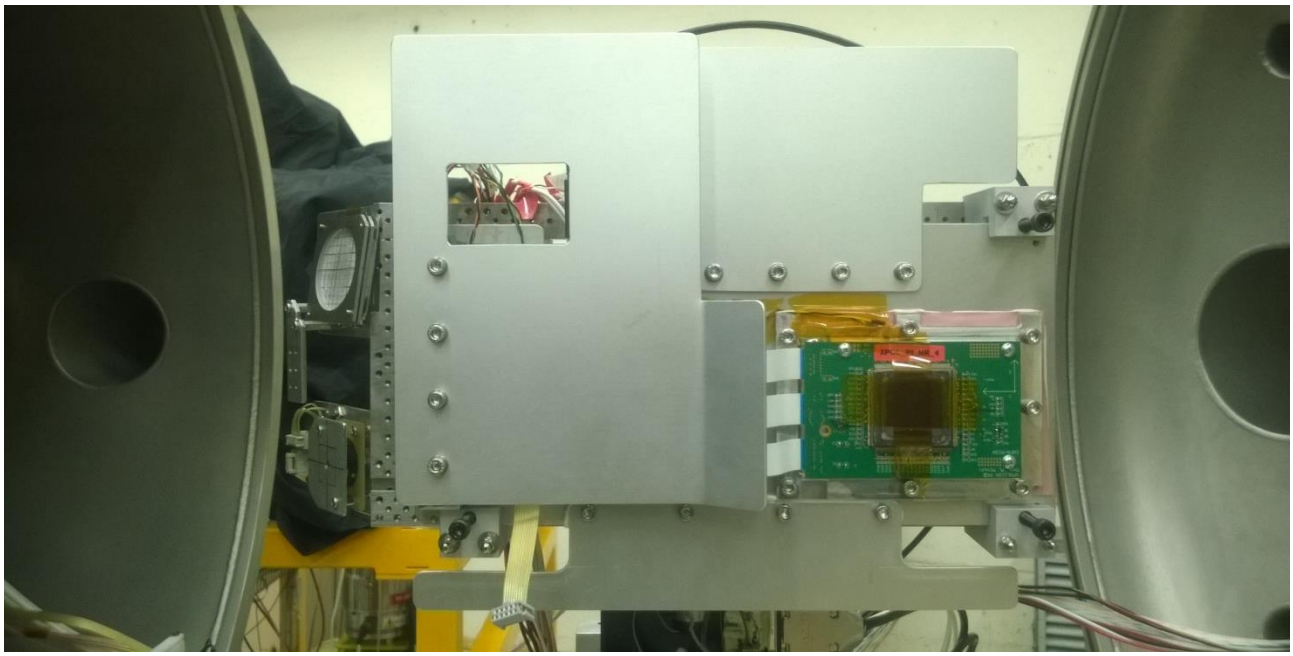

Figure 2: Picture of the holding structure for the test, fixed to the SIRAD holder

The irradiation was performed in vacuum at a typical pressure inside the SIRAD experimental chamber smaller than 10^{-5} mbar. We fixed the two boards composing the DAQ, the one with the power supply and the one with the FPGA, to a custom designed holding structure, shown in Figure 2. To dissipate the heat of the ASIC, FPGA and power supply board, we designed a set of radiators, shown in Figure 2. We included in the Arduino board a circuit to connect five PT-1000 thermocouples to monitor, with a sampling time of 10 seconds, the temperature of:

1. The ASIC XPOL,
2. The FPGA,
3. The A/D Converter,
4. The 1.8 V DC-DC converter,
5. The 3.3 V DC-DC converter.

The Arduino board was powered via the USB connector of a laptop.

2.2.4 Single Event Latch-up cross section

The latch-up cross section is measured separately for each ion. If $N_{latch\text{-}up}$ is the number of detected latch-up events, Φ is the incident ion fluence and θ is the angle of the ion beam from the direction orthogonal to the ASIC surface, the cross section is measured as

$$\sigma_{latch\text{-}up} = N_{latch\text{-}up} / \Phi_{effective} \quad (1)$$

$$\Phi_{effective} = \Phi \times \cos(\theta) \quad (2)$$

We recorded two latch-up events: one during the irradiation with ^{127}I and the other with ^{19}F. In both cases the current monitor powered off the ASIC, which recovered at nominal functionality when was powered on again after the idle time. The Arduino board controlling the current monitor gave an error message non consistent with a latch-up event. In both cases (^{127}I and ^{19}F), we continued the irradiation with the same configuration (ion, energy and LET) and we did not record any other latch-up. The fluence after detecting the latch-up was 1.34×10^{8} cm^{-2} for ^{127}I and 1.62×10^{9} cm^{-2} for ^{19}F respectively. A summary of the results is shown in Table 2.

Table 2: Results of the latch-up. $\Phi_{effective}$ is corrected for the effect of cos(θ) as in Eq. (2).

Ion	Rotation angle [deg]	LET [MeV cm^2 mg^{-1}]	$N_{latch\text{-}up}$	$\Phi_{effective}$ [cm^{-2}]	Cross section [cm^2]
^{19}F	0	3.9	1	1.96×10^{9}	5.10×10^{-10}
^{127}I	0	65.4	1	2.06×10^{8}	4.83×10^{-9}

After the irradiation, in the laboratory of INFN-Pisa we connected the ASIC to the current monitor and, during 24 hours of continuous testing, we detected 10 latch-up events. Again, the current monitor gave an error message of overcurrent protection when detected these latch-up events. We explain these events as given by fluctuations in the power supply of the Arduino board, powered via the USB connector of the same laptop used at SIRAD. Indeed, repeating the same test in the laboratory of INFN-Pisa and connecting the Arduino board to a stable power source we detected zero latch-up events during 48 hours of continuous test.

Although the detected latch-up events are unlikely and are most probably due to temporary fluctuations of the Arduino board, to be conservative we assume that they are real events and we estimate the expected rate in Sec. 2.3.1.

2.2.5 Single Event Upset cross section

Similarly to the $\sigma_{latch\text{-}up}$, separately for each ion we measure the cross section of the SEU in the memory registers ($\sigma_{SEU\text{-}REG}$) and in the pedestal scan ($\sigma_{SEU\text{-}PED}$) as

$$\sigma_{SEU\text{-}REG} = N_{SEU\text{-}REG} / \Phi_{effective} \quad (3)$$

$$\sigma_{SEU\text{-}PED} = N_{SEU\text{-}PED} / \Phi_{effective} \quad (4)$$

where $N_{SEU\text{-}REG}$ is the number of detected SEU events in the registers readout, $N_{SEU\text{-}PED}$ is the number of detected SEU events in the pedestal scan, $\Phi_{effective}$ is computed as in Eq. (2) from the incident ion fluence and the angle of the ion beam from the direction orthogonal to the ASIC surface. The results of the irradiation to measure the SEU in the memory registers are listed in Table 3 and shown in Figure 3.

Table 3: Results of the SEU of the bit in the memory registers. $\Phi_{effective}$ is corrected for the effect of cos(θ) as in Eq. (2).

Ion	Rotation angle [deg]	LET [MeV cm^2 mg^{-1}]	$N_{SEU\text{-}REG}$	$\Phi_{effective}$ [cm^{-2}]	Cross section [cm^2]
^{19}F	0	3.9	61	2.68×10^8	2.3×10^{-7}
^{19}F	30	4.5	72	2.54×10^8	2.8×10^{-7}
^{19}F	45	5.5	70	2.13×10^8	3.3×10^{-7}
^{35}Cl	0	12.7	70	8.84×10^7	7.9×10^{-7}
^{35}Cl	45	18.0	27	2.98×10^7	9.1×10^{-7}
^{79}Br	0	41.9	100	5.98×10^7	1.7×10^{-6}
^{79}Br	30	48.4	104	5.78×10^7	1.8×10^{-6}
^{79}Br	45	59.3	100	5.73×10^7	1.7×10^{-6}
^{127}I	0	65.4	371	1.99×10^8	1.9×10^{-6}
^{127}I	45	92.5	116	6.56×10^7	1.8×10^{-6}

We fit the cross section σ as a function of *LET* using a Weibull function:

$$\sigma = \sigma_\infty \left(1 - exp\left[-\left(\frac{LET - LET_{threshold}}{W}\right)^S\right]\right) \text{ if } LET \geq LET_{threshold} \quad (5)$$

In the fit we assume an uncertainty of 10 % on the fluence and a Poisson distribution for the number of SEUs. With these assumptions we find that $LET_{threshold}$ is consistent with zero, $\sigma_\infty = (1.9 \pm 0.2) \times 10^{-6}$ cm^2, W = 21.9 ± 5.5 and S = 1.2 ± 0.2 .

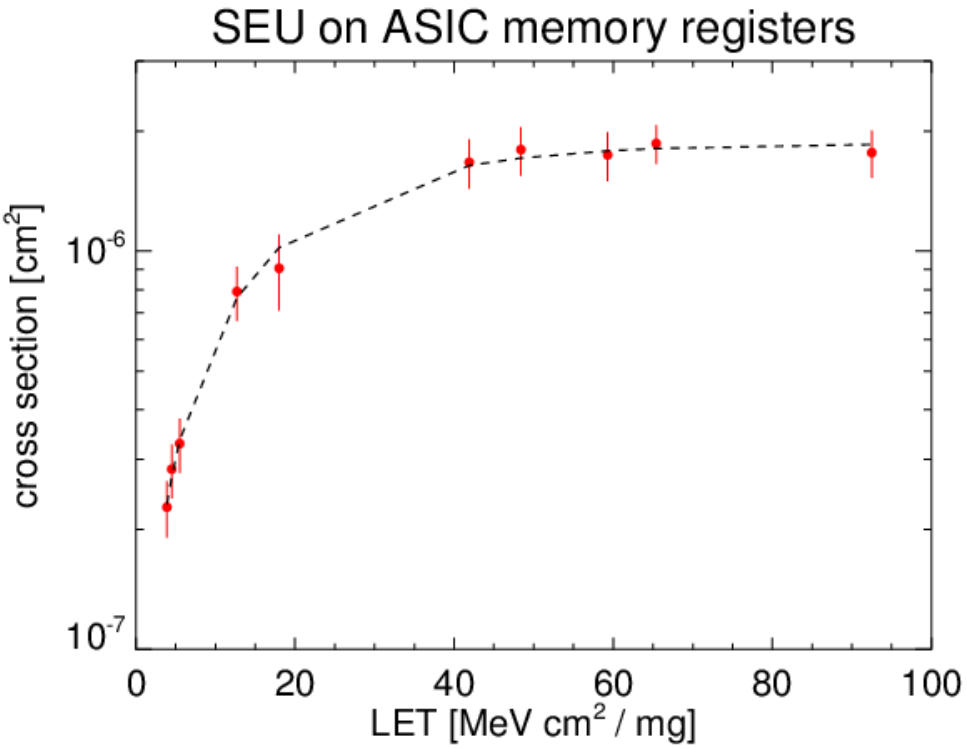

Figure 3: Cross section of SEU on the ASIC memory registers. Superimposed is the fit with the Weibull function.

The results of the irradiation to measure the cross section of the SEU during the pedestal scan are listed in Table 4 and shown in Figure 4.

Table 4: Results of the SEU during the pedestal scan. $\Phi_{effective}$ is corrected for the effect of cos(θ) as in Eq. (2).

Ion	Rotation angle [deg]	LET [MeV cm² mg⁻¹]	$N_{SEU-PED}$	$\Phi_{effective}$ [cm⁻²]	Cross section [cm²]
^{19}F	0	3.9	138	6.59×10^{7}	2.1×10^{-6}
^{35}Cl	0	12.7	127	1.73×10^{7}	7.3×10^{-6}
^{35}Cl	45	18.0	128	1.12×10^{7}	1.1×10^{-5}
^{79}Br	0	41.9	354	3.18×10^{7}	1.1×10^{-5}
^{79}Br	30	48.4	250	2.09×10^{7}	1.2×10^{-5}
^{79}Br	45	59.3	104	6.46×10^{6}	1.6×10^{-5}
^{127}I	0	65.4	87	7.29×10^{6}	1.2×10^{-5}

Similarly to the SEU on the memory registers, we fit the cross section σ as a function of LET using a Weibull function. Again we assume an uncertainty of 10 % on the fluence and a Poisson distribution for the number of SEUs. With these assumptions we find that $LET_{threshold}$ is consistent with zero, $\sigma_\infty = (1.21 \pm 0.08) \times 10^{-5}$ cm², W = 12.3 ± 1.9 and S = 1.5 ± 0.2 .

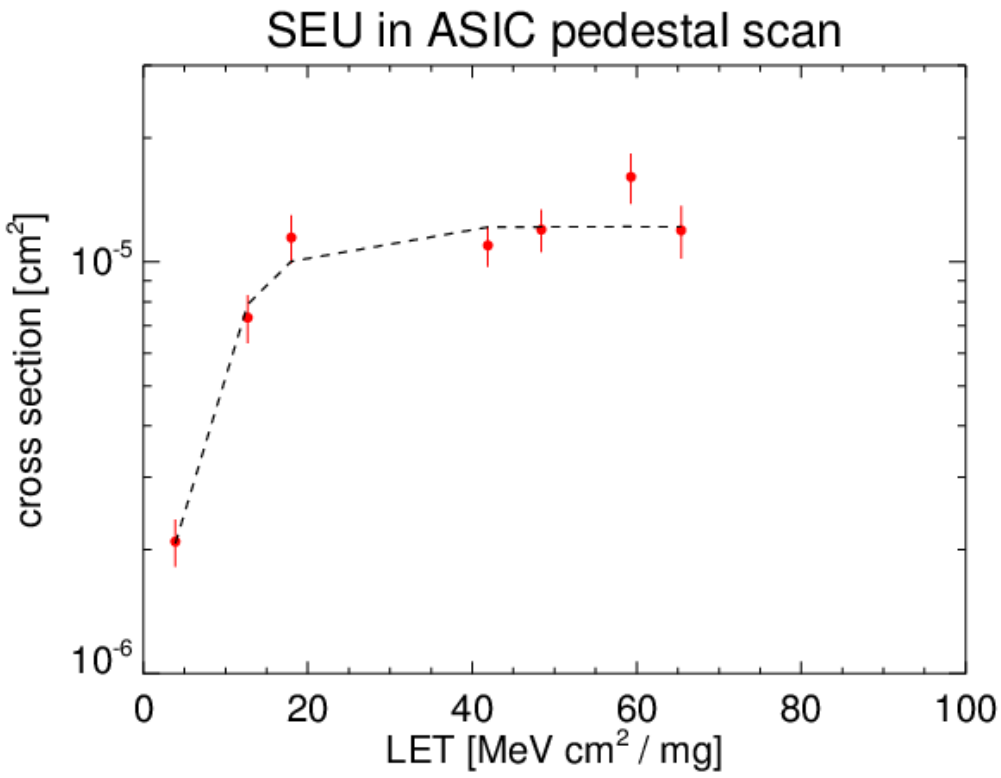

Figure 4: Cross section of SEU on the token which addresses the channel in the pedestal scan. Superimposed is the fit with the Weibull function. The LET axis has the same boundaries as in Figure 3.

2.2.6 Effects of the Total Ionising Dose

2.2.6.1 Effects on the functionality

The ASIC is still functional after receiving a TID above 500 krad.

2.2.6.2 Effects on the performance

Periodically during the irradiation, we measured the electronic noise from the distribution of the pedestals of the channels and the linearity using a charge injection technique.

We show in Figure 5 the distribution of the amplitude of the pedestals before starting the irradiation (green histogram) and at a dose level of ~200 krad (blue histogram). The increase of electronic noise is within 20 % at ~200 krad, with negligible effects on the GPD energy resolution (see Figure 5).

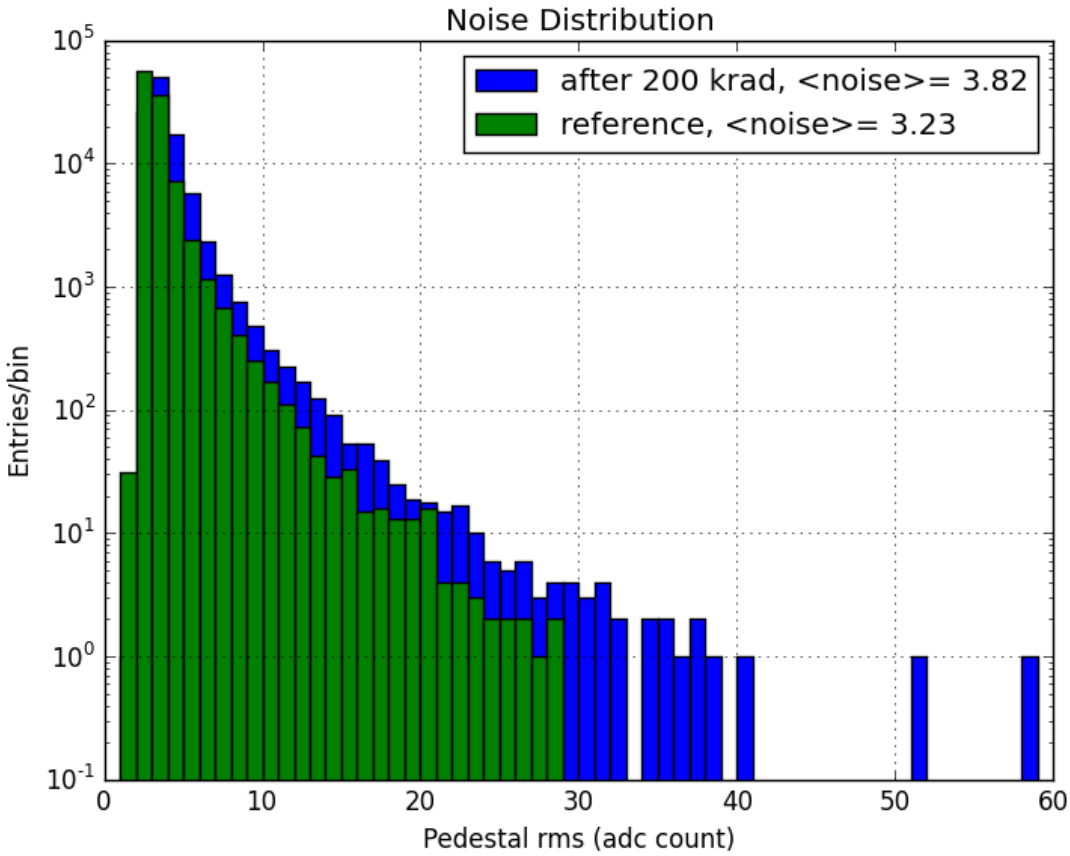

Figure 5: Variation of the electronic noise at 200 krad. The histogram in green is before starting the irradiation. The histogram in blue is at a TID level of 200 krad.

In addition, we measured the linearity of a sample of ASIC channels by charge injection. We show the superposition of the measured amplitude (in ADC channels) for different charge injected values (in DAC) on channels (150, 176), (68, 50) and (280, 332) at a dose level of ~400 krad (see Figure 6).

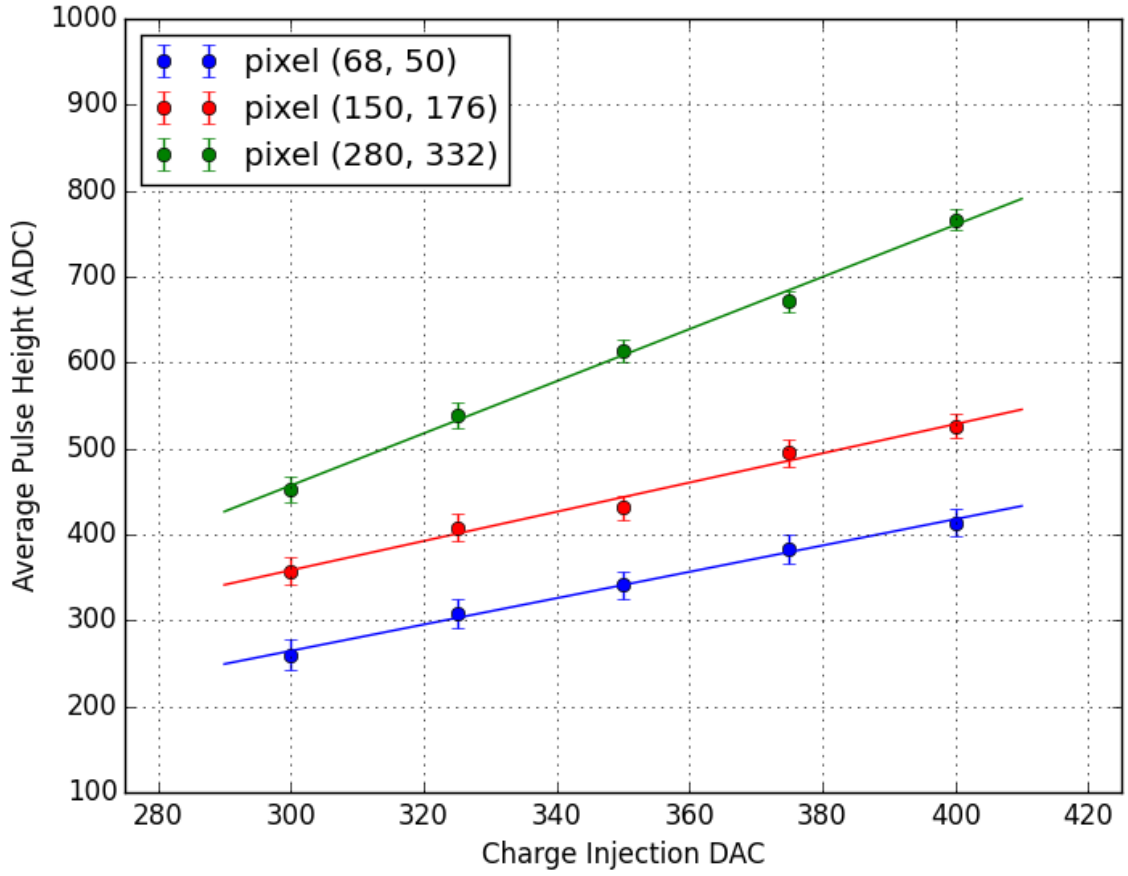

Figure 6: Linearity of the ASIC after receiving a TID of ~400 krad.

2.3 Expected rates in orbit and mitigation strategy

To estimate the expected rate of latch-up and SEU in orbit, we start from the expected LET spectrum of cosmic rays, trapped protons and worst 5 minute average Solar protons as listed in [AD1] assuming a shielding equivalent to 1 g/cm^2 of Al. The LET spectrum specified above from [AD1] is shown in Table 5.

Table 5: Cosmic ray, Trapped proton and worst 5 minute average solar proton LET spectrum calculated for the XIPE orbit (from [AD1]).

LET [MeV cm^2 / g]	Integral flux [particles/m^2/s/sr]	Differential flux [particles/m^2/s/sr/(MeV cm^2 / g)]
1	9.00×10^{3}	0
2	9.00×10^{3}	0
5	4.71×10^{3}	1.33×10^{3}
7	2.93×10^{3}	5.67×10^{2}
10	1.73×10^{3}	2.19×10^{2}
20	5.17×10^{2}	5.86×10
50	7.14×10	2.76
70	3.29×10	8.50×10^{-1}
100	1.46×10	2.98×10^{-1}
200	2.77	3.91×10^{-2}
500	8.11×10^{-2}	6.15×10^{-5}
700	6.96×10^{-2}	2.62×10^{-4}
1000	4.98×10^{-2}	0

2000	8.09×10^{-6}	0
5000	1.41×10^{-6}	3.35×10^{-10}
7000	6.35×10^{-7}	1.28×10^{-10}
10000	2.15×10^{-7}	7.61×10^{-11}

It is worth mentioning here that the LET values in Table 5 are in MeV cm^2 / g, i.e. 1000 times lower than the values measured at the accelerator (in MeV cm^2 / mg as in Table 2, Table 3 and Table 4). Similarly, the fluxes units in Table 5 are in particles/m^2/s/sr, i.e. 10000 times lower than the units at the accelerator (ions/cm^2/s, see Table 2, Table 3 and Table 4).

2.3.1 Latch-up

Although we are confident that the latch-up events detected during the irradiation at SIRAD are compatible with fluctuations in the power supply of the Arduino board, nevertheless we assume that these events are "real" to give a conservative estimation of the expected rate in orbit.

A very conservative upper limit of the expected rate of latch-up in orbit is obtained using the integral flux at 2000 MeV cm^2 / g (below the minimum value of LET used at the accelerator) and the cross section measured for the ^{127}I (highest value):

5×10^{-17} latch-up / s.

The solid angle is assumed as 4π sr. The mitigation strategy is represented by the introduction of a current monitor in the three BEEUs. This monitor is in charge of measuring the two currents of the ASIC (associated to the 1.8 V and 3.3 V voltages) in each GPD and to power off in case one of the currents exceeds a programmable threshold.

2.3.2 SEU

A very conservative upper limit is obtained by using the integral spectrum at 2000 MeV cm^2 / g (below the minimum value of LET used at the accelerator) and the saturation cross section σ_∞ from the fit with the Weibull function (see Sec. 2.2.5). We assume a solid angle of 4π sr. With these assumptions we obtain the expected rates:

- Pedestal scan (PED): 10^{-13} SEU / s;
- Registers (REG): 2×10^{-14} SEU / s.

As a mitigation strategy, we plan to reconfigure periodically the ASIC to prevent the corruption of the information in the memory registers due to a SEU. To mitigate the possible effect of a SEU in the pedestal scan, we plan to identify the corrupted events (with pulse height zero or saturated) and to exclude them from the analysis.

3 Environmental tests

During the preparation of the XIPE proposal a GPD prototype, serial number 014, of the has been extensively tested in laboratory and in space-like environment in an X-ray beam test [RD5]. In these tests we are evaluating the performance (most notably the gain stability) in a thermally controlled environment, both at atmospheric pressure and in vacuum.
The operational minimum and maximal temperatures in space are expected to be +5 °C and +25 °C. The minimum and maximum test cycle temperatures are chosen between -15 °C and +45 °C.

The following section of this document describes the result of the thermal-cycle and of the thermal-vacuum test.

3.1 The thermal-vacuum test

The test was performed in a thermal--vacuum chamber of our own construction. A vacuum vessel, 250 mm diameter, is mounted around the cold head of a CRYODINE cryostat. An aluminum flange is screwed on top of the cryostat head. On the lower face of the flange there are 4 resistors of 10 Ω each, connected in series to a computer-controlled power supply, configured to provide a voltage up to 50 V. While the cold head is always on, the resistors act in competition with the cryostat freezing and provide the required power to rise the temperature and to keep it constant when necessary.

The detector is mounted over the top face of the flange and a thermal conductive sheet guarantees a good thermal connection. A PT1000 temperature sensor is attached with aluminum tape over the detector base frame in direct contact with the aluminum flange (control sensor, used as reference temperature in this test). A LabView program is used to read the PT1000 temperature (via a NI 9219 analog input module) and to change the voltage across the heating resistors.

The vessel is connected to a Varian 979 leak detector system that is actually used as vacuum pump. During the test the pressure inside the vessel was monitored with a Pfeiffer PKR 251 vacuum gauge. A picture of the test setup is shown in Figure 7, while Figure 8 shows the thermal--vacuum chamber and the detector with its connections.

A single +45 °C, -15 °C cycle at P ~ 2-3 x 10^4 mbar was performed as shown in Figure 9. The detector was successfully tested collecting X-ray events from a ^{55}Fe circular source, diameter 1 cm, placed on top of the detector entrance window. We performed 4 data acquisitions, at 15 °C at the beginning and at the end of the cycle, at the highest operative temperature (20 °C) and at the lowest operative temperature (10 °C). We studied the gain of the detector (defined here as the peak of the pulse height distribution) and its stability, finding a maximum variation of less than 1%. The energy resolution was also studied, finding a stable result of ~20% FHWM. Figure 10 shows an example of the pulse height distribution for the last data acquisition in this test.

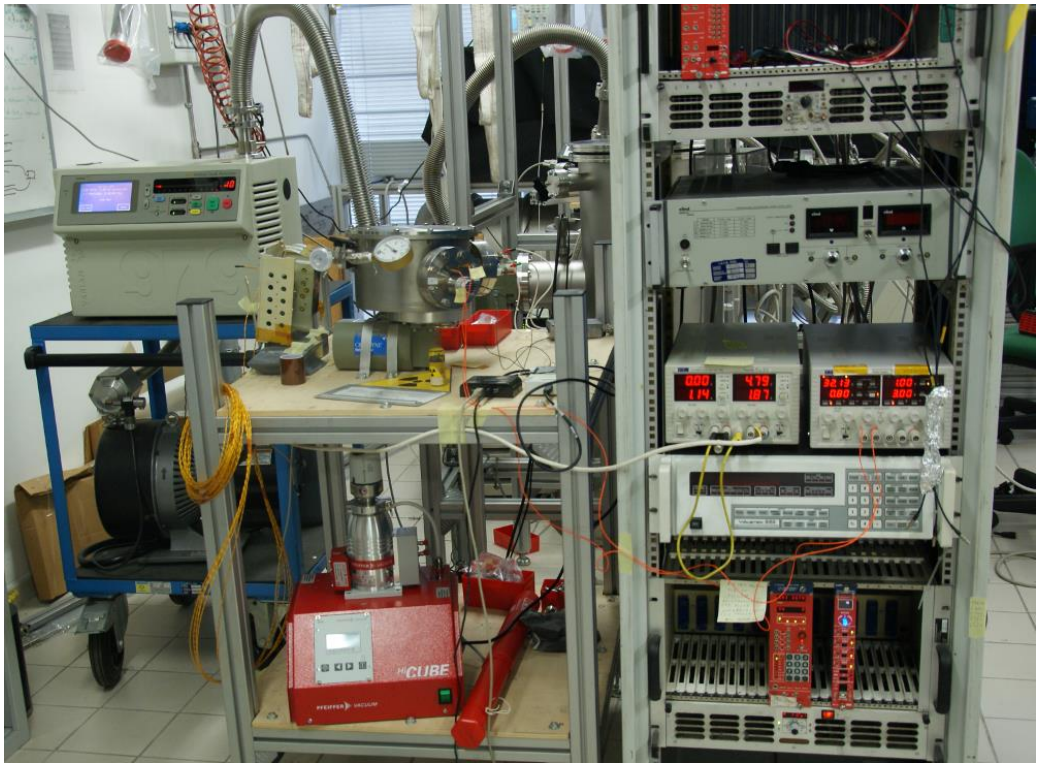

Figure 7 Picture of the test setup, showing the vacuum pump (on the left), the vacuum vessel (on the table in the center of the picture) on top of the cryostat, and the rack with high-voltage and low/voltage power supply (for detector and heaters).

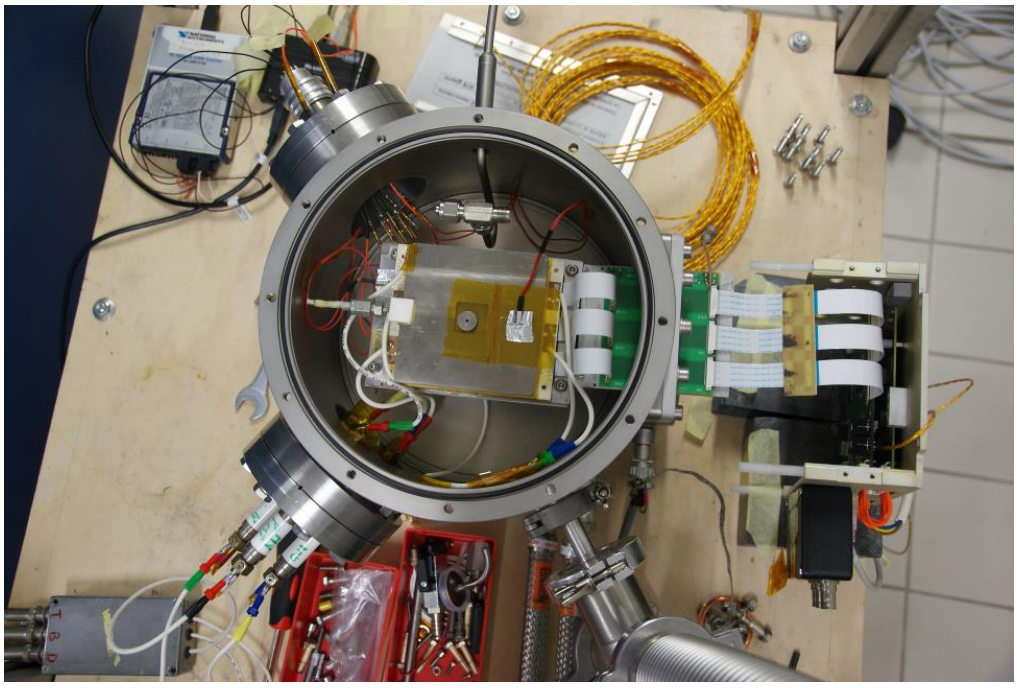

Figure 8 Picture of the thermal-vacuum chamber during the test preparation. The detector is visible inside the vessel, with the ^{55}Fe radioactive source on top of the entrance window (protected with Kapton tape). The 3 white, flat cables connect the detector to its control board, visible on the right side of the picture. The high-voltage feedthrough is visible at the bottom-left of the picture while the heaters and temperature monitor feedthrough are on the top-left. The vacuum pump and the pressure sensor are connected to the flange on the bottom-right of the vessel.

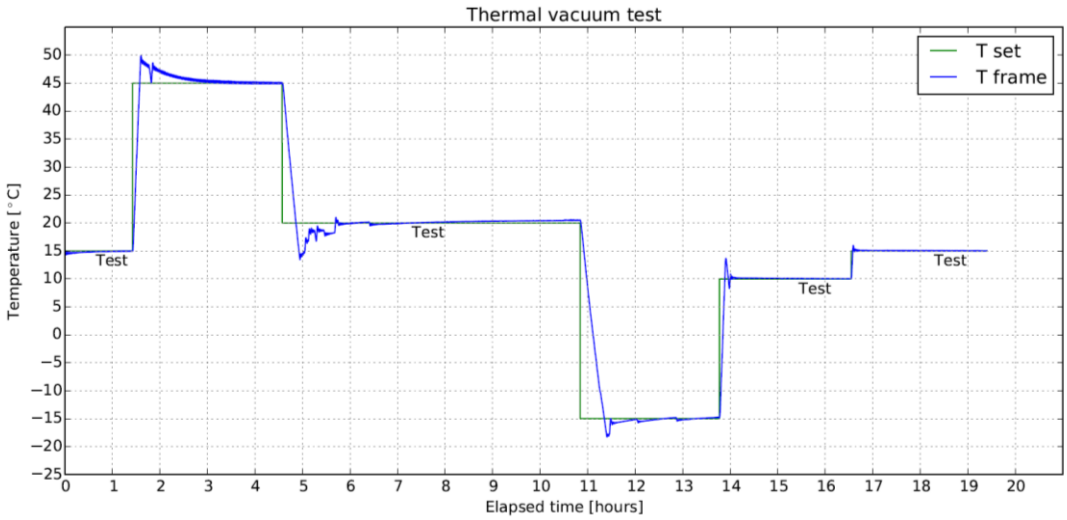

Figure 9 Plot of the temperatures profile of the thermal-vacuum test. Planned temperature is shown in green, while the temperature measured on the base frame of the detector in direct contact with the cryostat head and with the heating resistors is in blue. The approximate time of detector test is also indicated in the figure.

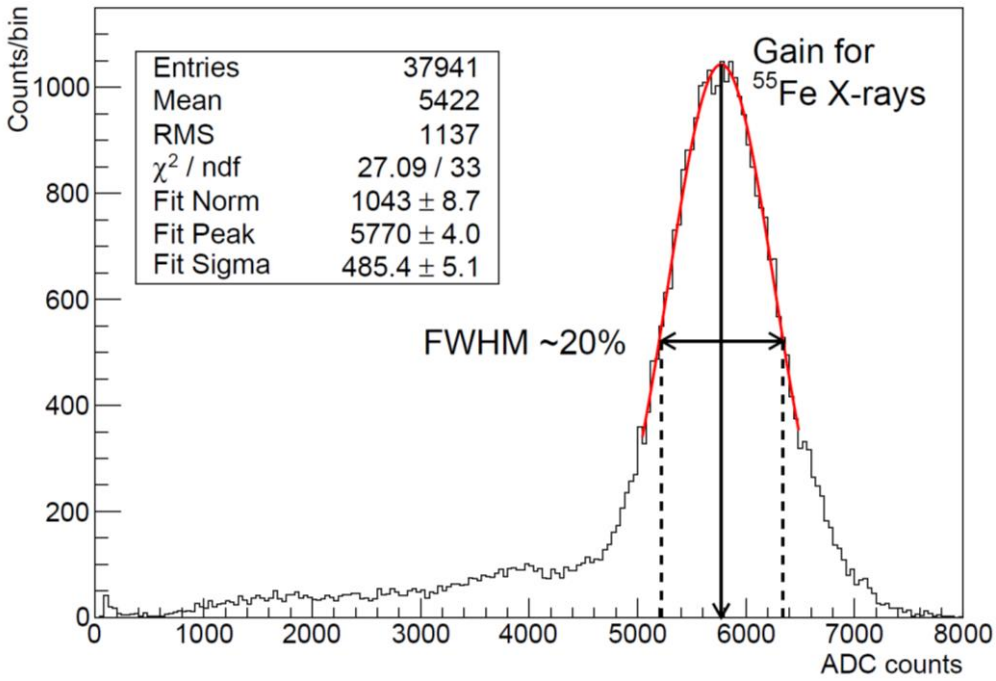

Figure 10 Pulse height distribution for ^{55}Fe photons collected during final plateau at 15 °C. Peak value and energy resolution are also indicated.

3.2 The thermal cycle test

The test was performed in a computer-controlled climatic chamber Angelantoni Hygros 600 at Teslab S.r.l. The temperatures where recorded with 3 thermocouples (in addition to the chamber control), two were connected to the base frame and top window of the GPD and one monitors the air temperature near the detector. Figure 11 and Figure 12 show the test setup. A ^{55}Fe circular source, the same one used in the thermal-vacuum test, is placed on top of the entrance windows.

In Figure 13 the graphs of the thermocouples temperatures are shown. The detector was turned on during the first 3 plateaus at 15, 20 and 10 °C and X-ray data were collected. The gain and the energy resolution where studied finding a gain variation of about 1% and a stable energy resolution of ~ 20% FHWM.

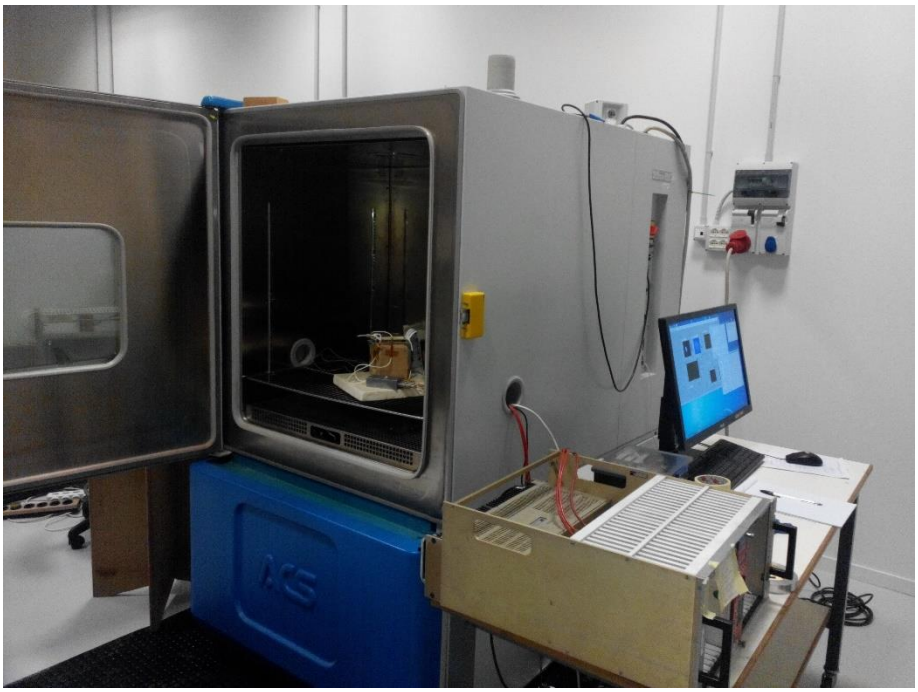

Figure 11 Picture of the test setup, showing the thermal chamber with the detector during the test preparation and the polarimeter control hardware: the PC and the high-voltage power supply (the low-voltage power supply is not visible).

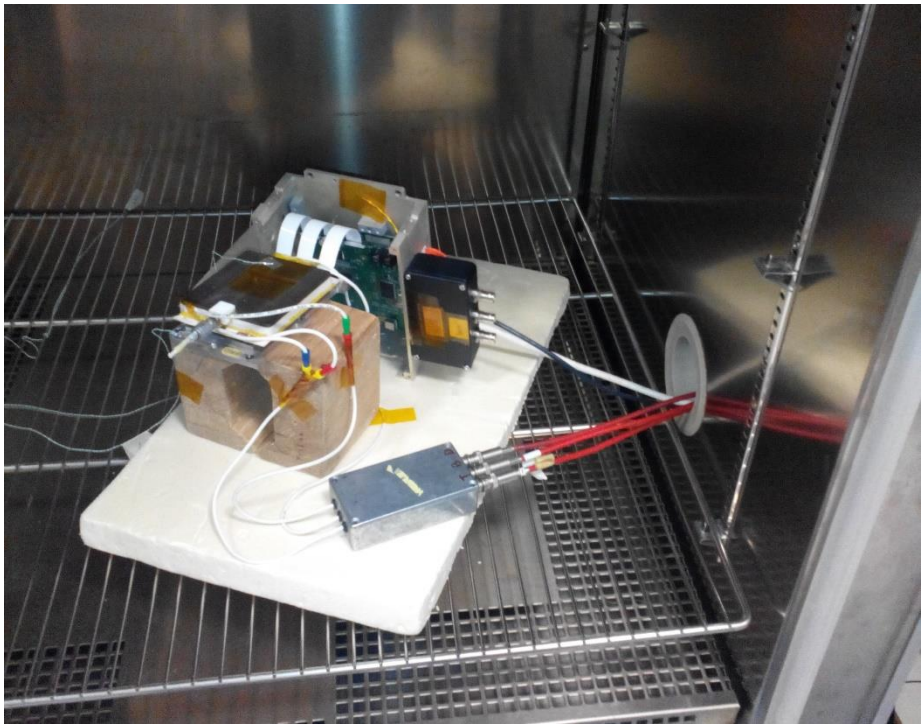

Figure 12 Picture of the polarimeter inside the thermal chamber. The detector is visible in the front, while the DAQ board are on the back of the picture (connected via the white at cables). The three thermocouples (at the end of the green-white small wires on the left side) are also visible.

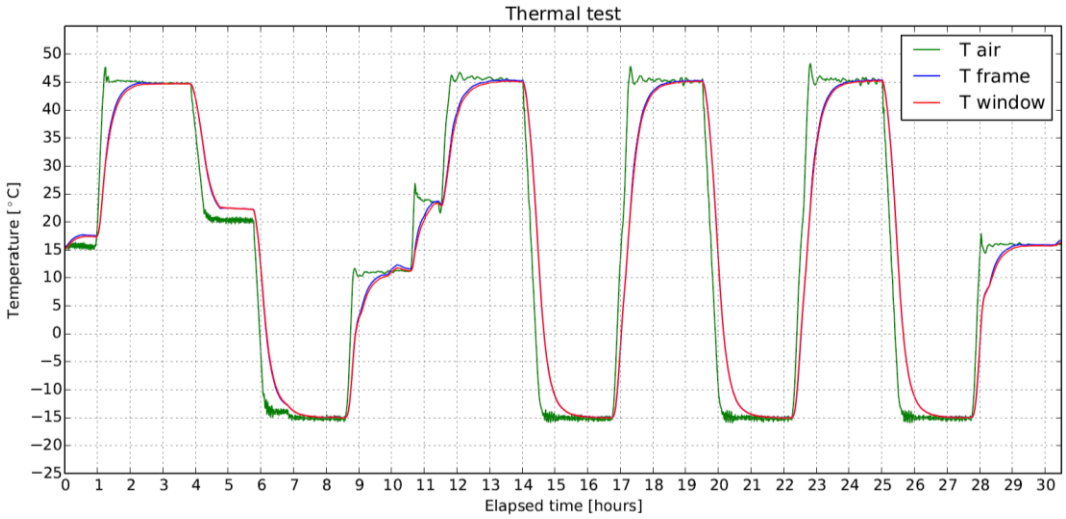

Figure 13 Plot of the thermocouples temperatures profile during the test. Air temperature is shown in green, while the temperature measured on the base frame of the detector is in blue while the one on the top window in red. The detector was tested at 15, 20 and 10 °C.

4 Vibration test

A vibration test was performed on GPD prototype 014 to check resonance frequency and verify its mechanical integrity.

4.1 Test setup

Vibration test was performed in facility at TesLab s.r.l. (Livorno, Italy). The test equipment is described in the following table:

TesLab code number	Equipment	Manufacturer	Model
ST055S01	Vibrating table	LDS	730-335 + slip table 750x750
ST055S02	Amplifier	LDS	SPA 10/20K
ST067F	Monoaxial Accelerometer	Dytran	3055B4
ST247A	Digital controller	LDS Dactron	Laser USB
ST067F10	Reference accelerometer	Dytran	3055B4

For each axis we have performed:

1. First resonance search
2. Vibration Test: Random
3. Vibration test: sinusoidal
4. Second resonance search

A picture of the experimental setup is shown in Figure 14.

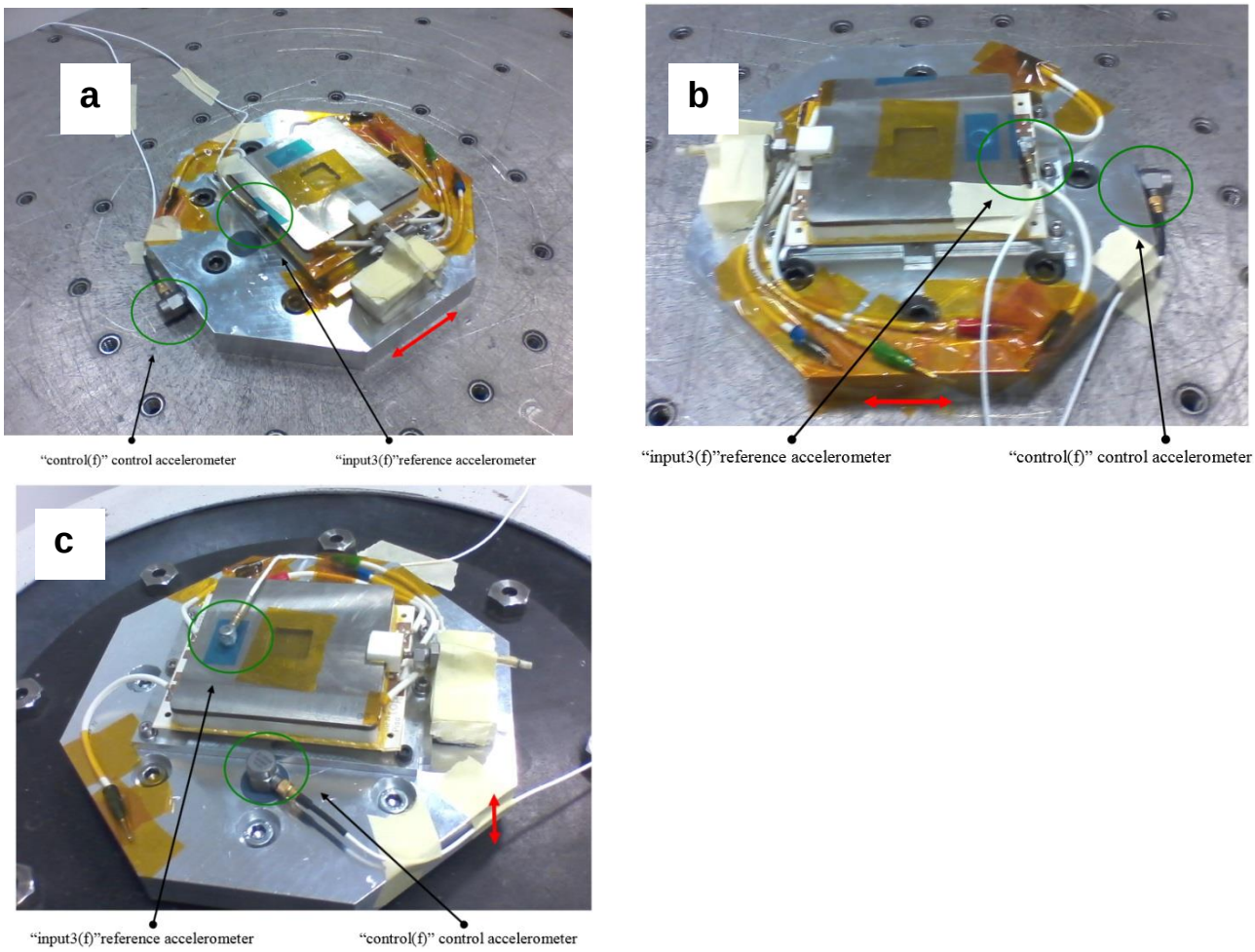

Figure 14 Vibration test experimental setup: : a) X axis; b) Y axis; c) Z axis

4.1.1 Resonance search method

Search of resonance peak was done, according to [RD8] with the following parameters:

Frequency Range:	5 Hz – 2000 Hz
Amplitude:	0.5 g
rate:	2oct/min

4.1.2 Random loads

Random loads applied for two minutes (from [RD6] Table 2.4-4, Component Minimum Workmanship Random Vibration Test Levels):

Frequency Range	5 ÷ 2000 Hz	
RMS value	Frequency (Hz)	ASD Level (ASD (g^2/Hz)
	20	0.01
	20 - 80	+3 db/oct
	80 – 500	0.04
	500 - 2000	-3 db/oct
	2000	0.01
	Overall	6.8 g rms

4.1.3 Sinusoidal loads

Sinusoidal loads are applied according to [RD7], as described in the following table:

Frequency Range	5 Hz – 100 Hz					
Description	AXIS	F(Hz)	Level (g)	F(Hz)	Level(g)	Rate (oct/min)
	X-Y	5-25	1	25-100	0.62	2
	Z	5-45	1	45-100	1.25	2

4.2 Test result

The test was performed on November 18, 2014. A summary table of the resonance search, before and after vibration test is in the following tables:

Resonance Number	Axis	Resonance Frequency [Hz]	Resonance Amplitude [gn]
1	X	1527	2
2	**X**	1758	2.9
3	**X**	1931	1.9
1	**Y**	577	0.7
2	**Y**	649	0.6
3	**Y**	1492	0.8
4	**Y**	1658	1.3
5	**Y**	2000	1
1	**Z**	551	4.4
2	**Z**	626	4.9

Resonance founded Number	Axis	Resonance Frequency [Hz]	Resonance Amplitude [gn]
1	X	1509	1.9
2	**X**	1758	3.3
3	**X**	1931	2.6
1	**Y**	557	0.7
2	**Y**	641	0.5
3	**Y**	1492	0.8
4	**Y**	1658	1.1
5	**Y**	2000	1
1	**Z**	513	4.3
2	**Z**	619	3.9

Notice that the resonance showed in the sine sweep test are mostly due to the gas felling tube that could not be removed of fixed, but is part of the prototype only, for testing purpose, and will not be present in the flight models.

The detector was tested with a ^{55}Fe source at the usual voltages after the random test showing the same stable performance as before the vibe test

The following figures show the results of the sine sweep, random and sinusoidal test for the X (Figure 15), Y (Figure 16) Z (Figure 17) axis.

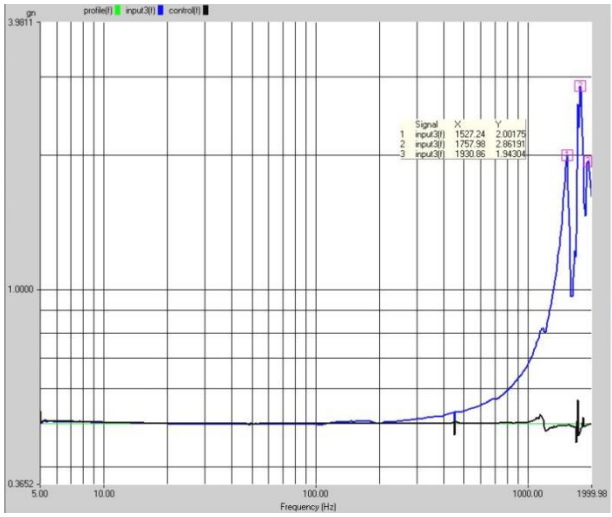

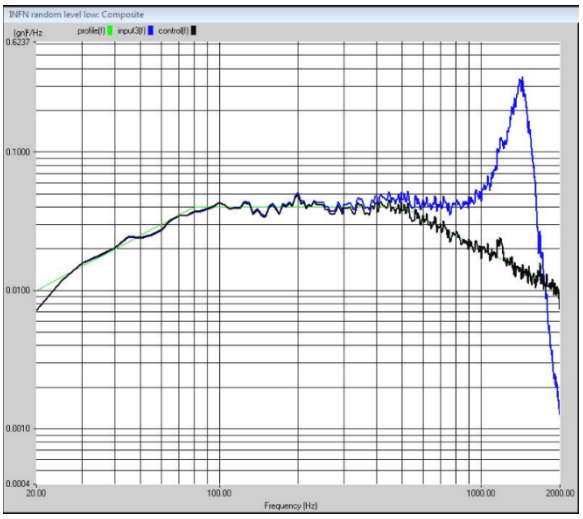

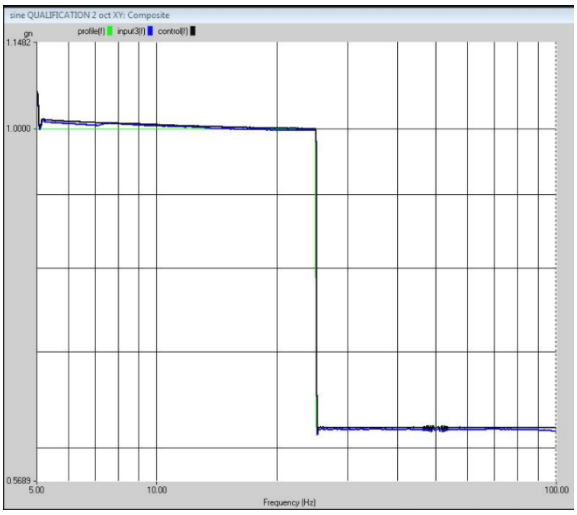

Figure 15 The sine sweep spectra, the random tests and the sinusoidal results for the X axis.

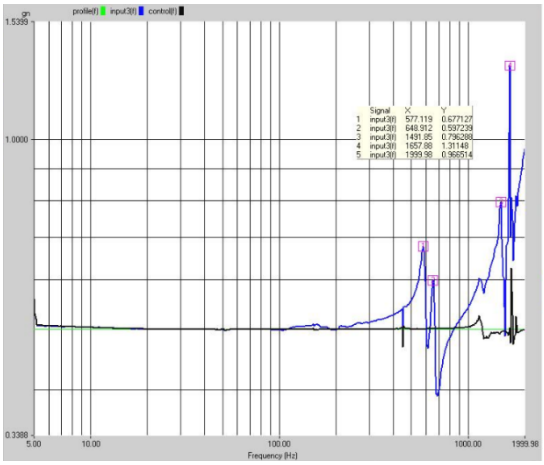

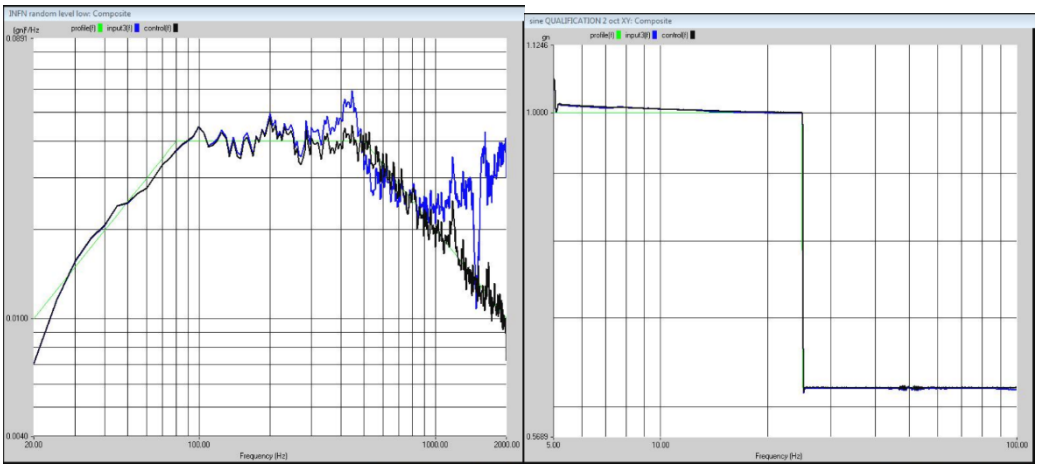

Figure 16 The sine sweep spectra, the random tests and the sinusoidal results for the Y axis.

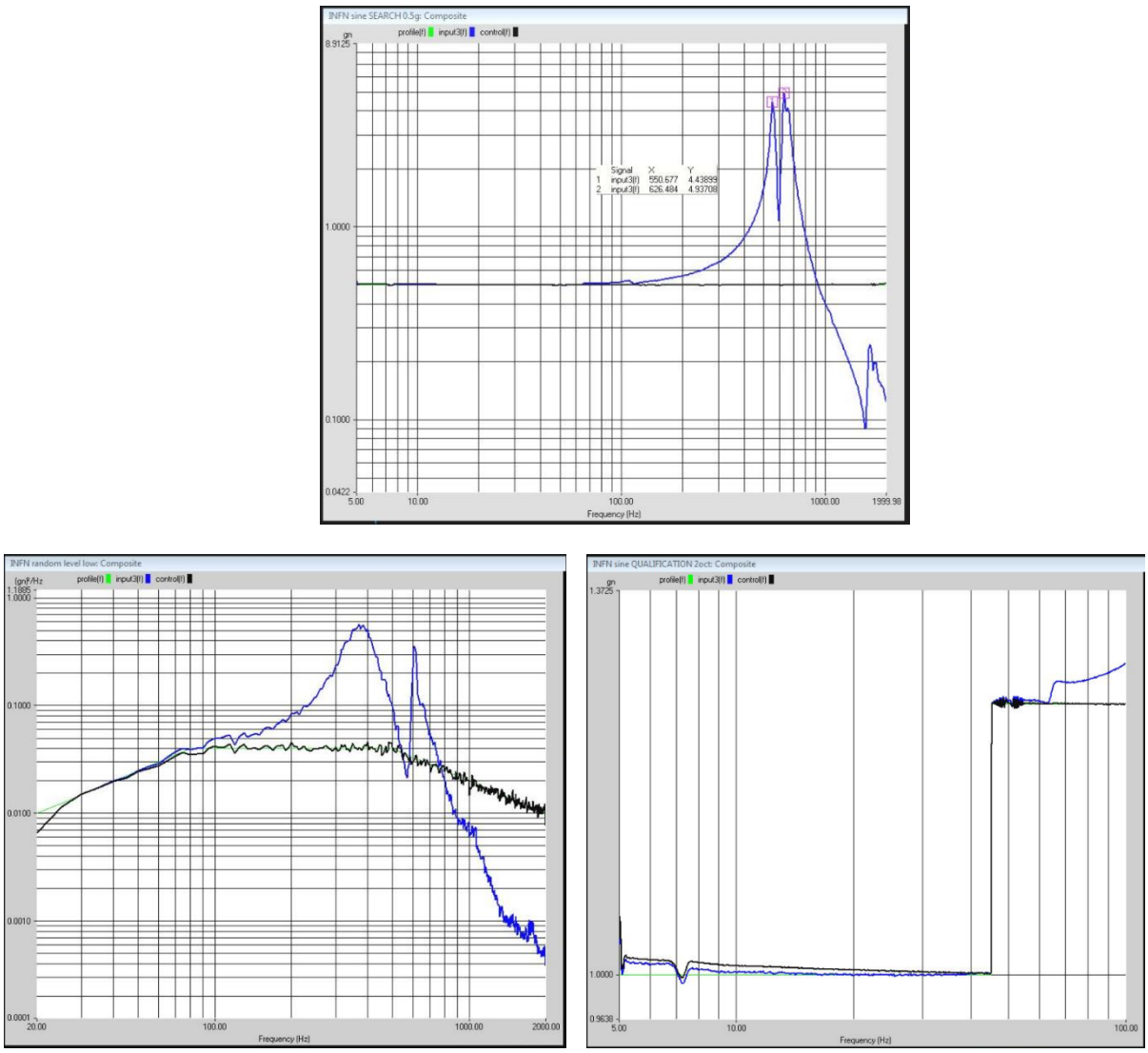

Figure 17 The sine sweep spectra, the random tests and the sinusoidal results for the Z axis.

5 Long duration leak test

This test aims at studying the gas leak rate as function of time, in order to check possible effect of the aging of the gas cell.

5.1 Test item

The test has been performed on the GPD with serial number 014, shown in Figure 18.

This test item is structural representative of the GPD design and is the only one currently not in use for electrical and performance test: in this way we minimized the impact of this long duration test on the prototype production schedule.

This GPD is equipped with a gas connector that facilitate connection of the gas cell to the leak detectors. In newer prototypes, the gas pipe is crimped after filling and need to be cut for refill or leak tested.

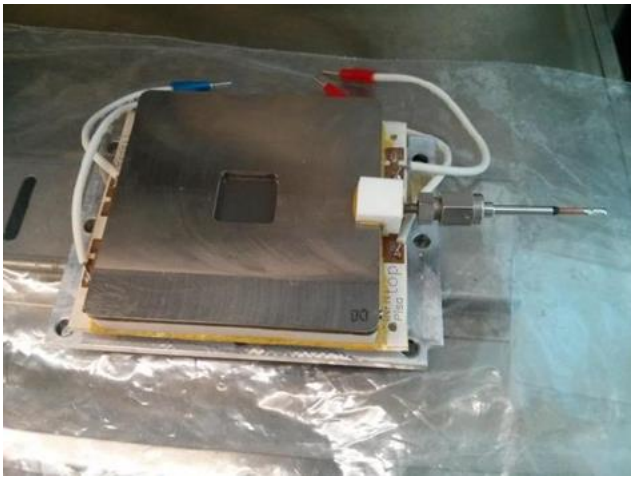

Figure 18 Picture of the GPD serial number 14, the Be window is protected by a plastic cover (to be removed during test), the gas tube and its connector is clearly visible.

5.2 Test method

The test has been using the facilities at the Oxford Instruments Analytical Oy (OIA) at Espoo (Finland).

The polarimeter detector was first found non-leaking with conventional He leak detection (leak rate <1e-9 mbar l/s). This method consists of flushing He on its outer surfaces, pumping and detecting He via the detector pump tube. A conventional He leak detector (as specified below) was used.

The detector was then filled and sealed with 1 atm He gas. The method to test this configuration was to put the sealed detector into a vacuum chamber, pump it down and by using a Residual Gas Analyser try to detect helium in the vacuum. The test period was specified to be > 3 weeks.

Figure 19 Picture of the GPD serial number 14 installed into the vacuum chamber (at OIA).

Equipment used:

- OIA custom built pumping and baking station
- Turbomolecular pump Varian V70LP
- Residual Gas Analyser Stanford Research Systems RGA200

- He leak detector Adixen ASM 142

5.3 Results

The empty chamber was first tested to get a base-line reading of the system. Then the detector was installed and measurements started. No clear He peak (m/e=4) could be detected above instrumental noise in normal scanning mode. It was therefore decided to scan for periods of 4h, to get an averaging over such a time frame. The raw data from the first 3 test occasions are shown in

Figure 20page5.

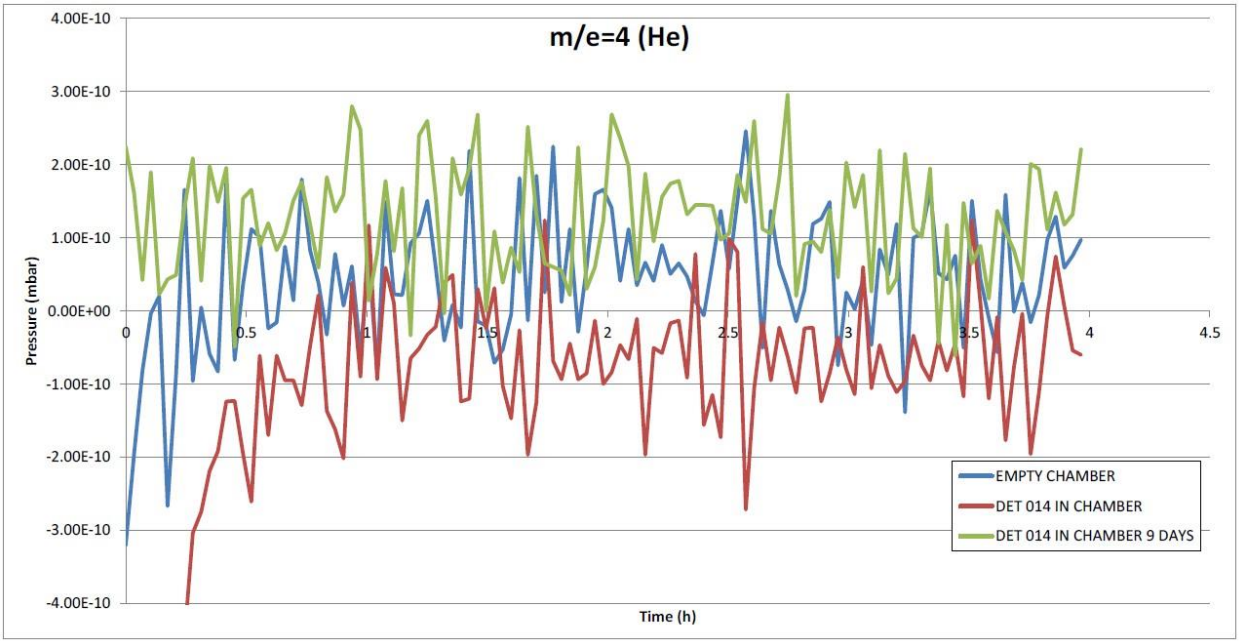

Figure 20 RGA raw data for the 3 first test occasions.

It can be seen that the first two occasions (red and blue lines) have clear pressure “transients” during first 1.5h or so. This must be because the measurement started immediately during the chamber pump down as soon as the total pressure was below the safe operating pressure (<10^{-4} torr). Since pressure cannot be negative, this must be an instrumental offset, which is depending on chamber total pressure. Because of this only the last 2h of the 4h test periods were used in averaging the results for each test occasion.

The averaging method results for the next 30 days of testing is shown in Figure 21.

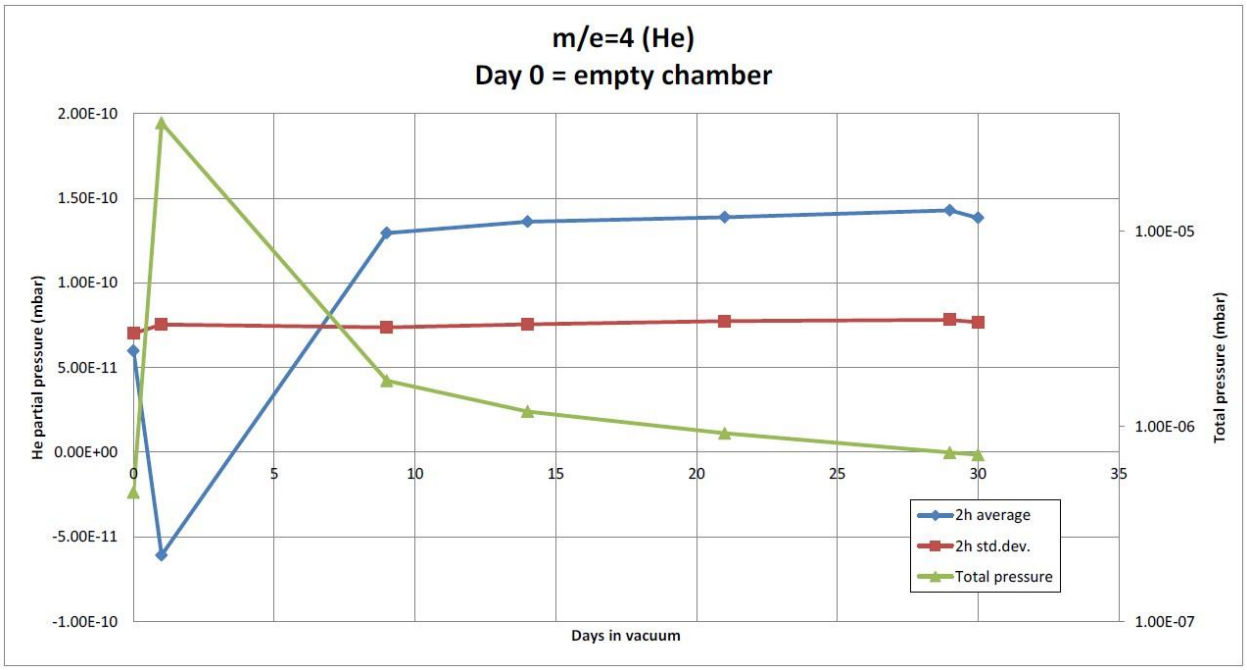

Figure 21 Averaging results for 30 days in the vacuum. Green line= chamber total pressure [mbar]; blue line= He partial pressure 2h average [mbar]; red line= He partial pressure std. dev. [mbar].

As can be seen there is actually a difference in the He peak pressure when comparing the empty chamber (day 0) with the other days, except day 1, which can be explained by the total pressure instrumental offset effect. When converting this pressure difference into corresponding leak rate, the earlier established effective pumping speed of He for the system (43 l/s, see [RD9]) must be used.

GPD Measured Leak Rate = (He pressure with detector – He pressure empty) x 43 = 8e-11 mbar x 43 l/s = 3.4e-9 mbar l/s

This measured leak rate value has no detectable effects on the GPD performances over the life span of the GPD for the XIPE mission. The corresponding DME gas pressure leak (= 0.3 x He leak = 1.02e-9 mbar l/s) during a period of more than 5 year is <0.1 mbar (see Figure 22), that means a DME gas pressure ratio < 0.1 / 800 mbar < 0.015%.

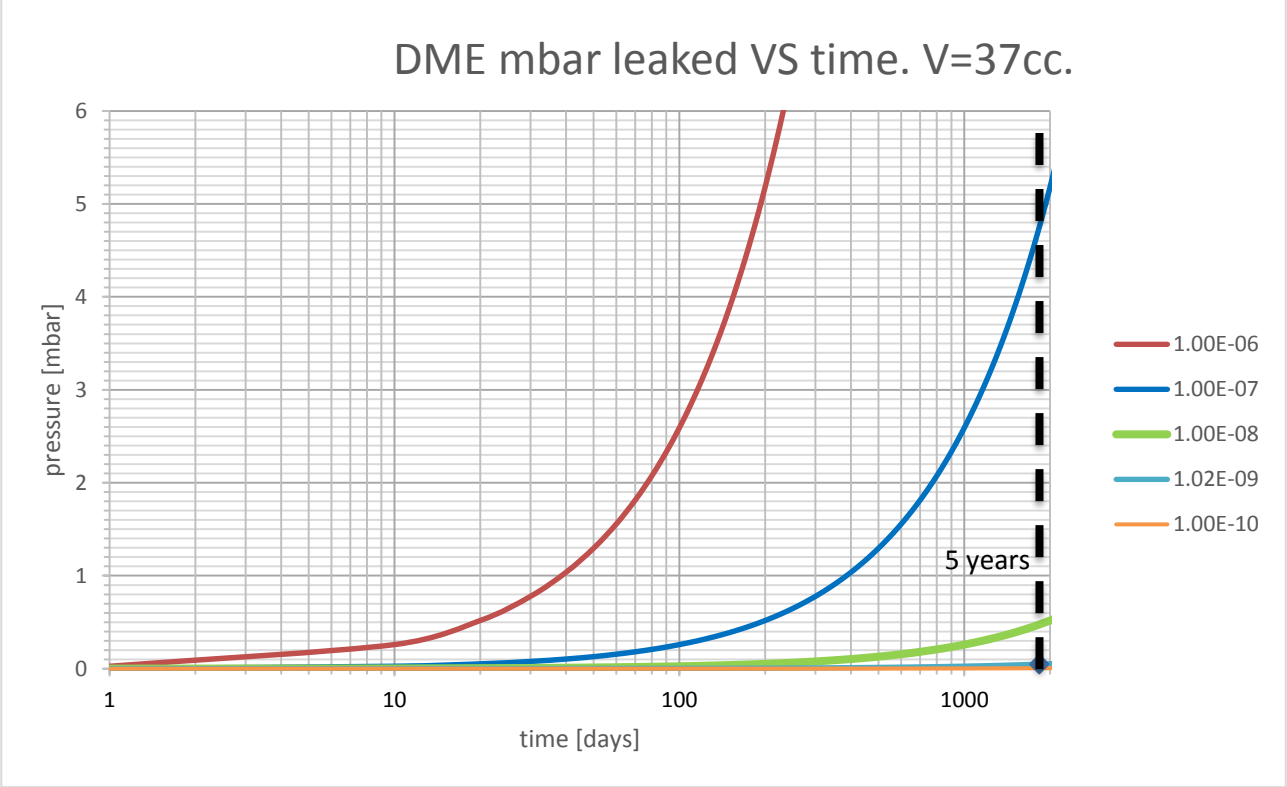

Figure 22 GPD gas mixture leaked (DME) during time for several leak rate values

Since the first (and only) measurement point of the empty chamber also suffered from the offset transient due to high total pressure, it was decided to double check the empty chamber reading. The detector was removed from the chamber and the empty chamber test was repeated for several days as shown in Figure 23.

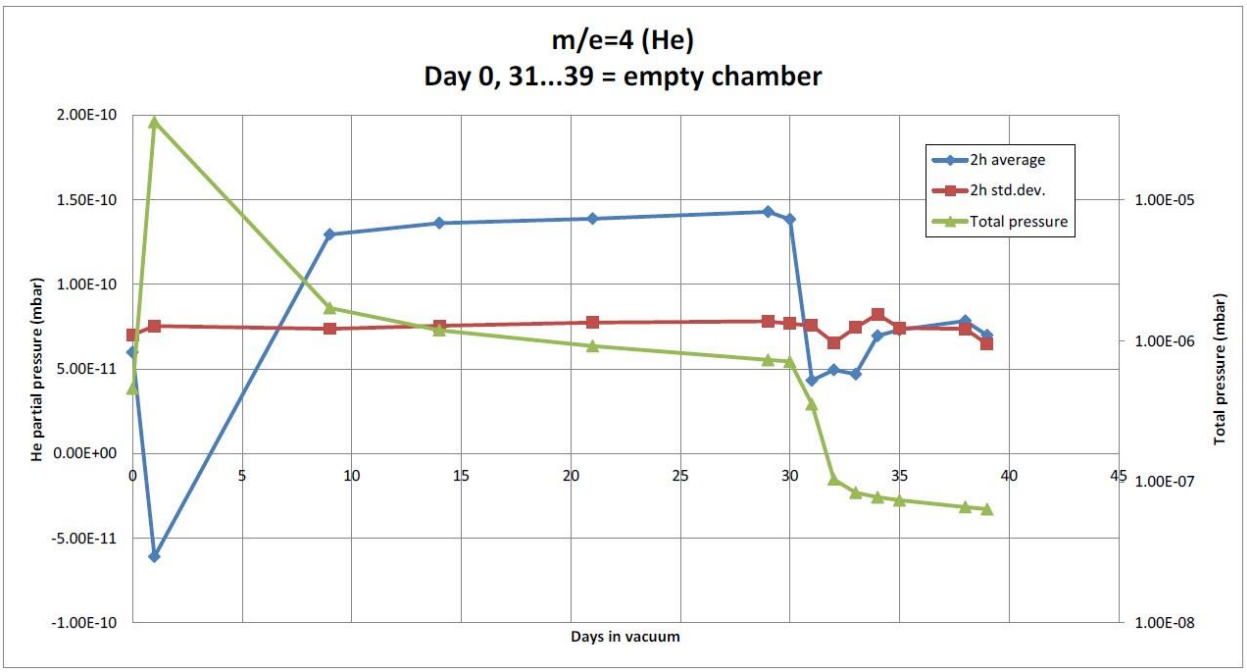

Figure 23 Additional days with empty chamber.

It can be seen that empty chamber pressure level remains on roughly the same level as the result from day0, so the leak calculated above is valid.

5.4 Conclusions

The GPD S/N 014 has been tested for long-term leak effects in vacuum environment. The He partial pressure that has been detected during the test is affected by instrumental offset and measurement errors that has been mitigated averaging the results. The calculated He leak rate of 3.4e-9 mbar l/s corresponds to a negligible gas mixture leak, so we can conclude that the GPD doesn't have any detectable degradation of its performance over its XIPE life span of more than 5 years.